Flow computation inside a scroll compressor based on open-source code

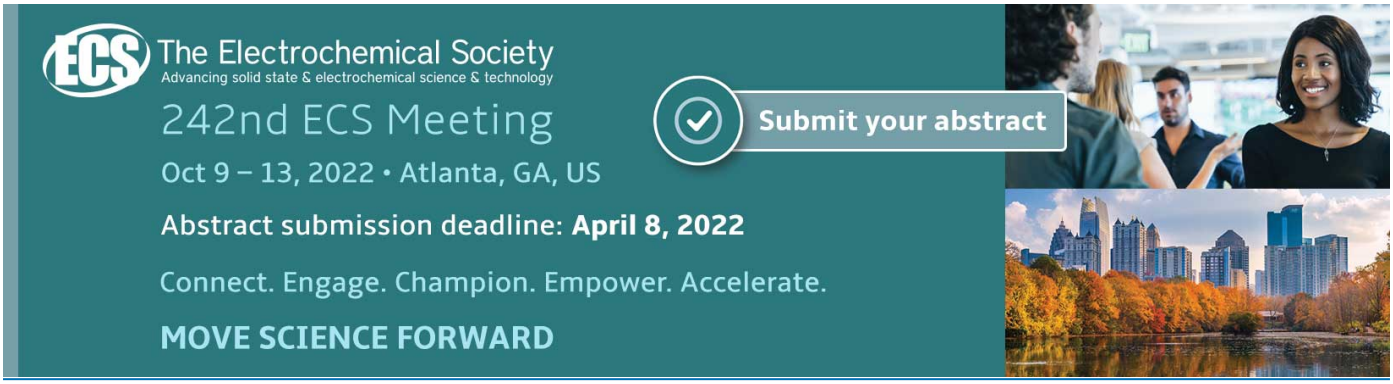

Flow computation inside a scroll compressor based on open-source code

E Fadiga[1], N Casari[1], B Angel[2], A Picavet[2]

[1] Department of Engineering, Università di Ferrara, Via Saragat 1, 44122 Ferrara, Italy
[2] Danfoss Commercial Compressors, Parc TECHNOLAND, 2 Allée Toscane, Zi du Champ Dolin, 69800 Saint-Priest, Francia

E-mail: ettore.fadiga@unife.it

Abstract. Computational fluid dynamics (CFD) is an essential tool for improving the performance of positive displacement machines, which are commonly adopted in vapour compression applications. The numerical analysis of such machines is characterized by several modelling challenges. Firstly, the relative motion of the wraps and the presence of particularly small gap sizes need to be considered during the implementation of a reliable meshing strategy. In addition to that, the operating conditions are close to the saturated-vapour line, requiring a real gas equation of state for the determination of fluid thermophysical properties.

In this work, a commercial scroll compressor has been simulated at three different operating conditions. The geometrical modelling, meshing strategy and compression process have been obtained thanks to a set of libraries built in OpenFOAM-v2006. The results have been compared with experimental data of the pressure evolution in the compression chambers. Furthermore, a complete fluid flow analysis is presented to assess the capabilities of the developed tool when applied to a compressor operating with R410a.

1. Introduction

Among positive displacement (PD) machines, the scroll compressor is a device largely employed in refrigeration systems and air conditioners since the 1980s. These machines have become one of the most commonly adopted compressors in such sectors, so it is important to study their dynamic behaviour to improve their overall performance.

The most common strategies to analyze scroll compressors are experimental campaigns [1–3], aided by theoretical studies [4, 5], semi-empirical modelling [6] and thermodynamic analyses [7, 8]. However, the flow inside positive displacement machines has a complex three-dimensional nature, especially in suction and discharge regions. Unfortunately, such flow features are either impossible or extremely costly to determine experimentally. Hence, Computational Fluid Dynamics (CFD) represents a suitable method to perform a complete analysis of the dynamic behaviour of positive displacement PD machines.

The majority of the works presented in the literature is based on the definition of a structured grid (in the scroll set), and the operation is simulated by means of pre-defined motion of the nodes. This method allows obtaining good accuracy reducing conservation errors, as extensively described in section 2. However, a number of works have been performed with re-meshing techniques [9, 10] or cartesian cut-cells methods [11, 12].

The analyses based on pre-defined mesh generation available in the literature are mainly realized using commercial CFD software. These software are usually coupled with mesh generators focused on positive displacement machines. In particular, the mesh generator *Twin Mesh* has been used by Hesse et al. [13] to simulate a scroll vacuum pump considering thermal deformation with ANSYS CFX. The same computational workflow has been applied by Picavet et al. [14, 15] to simulate the same compressors studied in this work, respectively with and without Intermediate Discharge Valves (IDVs). The mesh generator and CFD software SimericsMP+ has been used by Cavazzini et al. [16] to perform a CFD-based optimization and uncertainty quantification of a scroll compressor.

In this work, the authors have performed a full three dimensional CFD simulation of a commercial scroll compressor produced by Danfoss using open-source software. The numerical results, based on the framework developed by Fadiga et al. [17], have been experimentally validated using the data obtained by Picavet et al. [3]. In particular, the effects of the discharge region geometry on the convergence of the simulation have been investigated, as well as the gap size impact on leakage flows. The analyses conducted by Fadiga et al. in [17] and [18] along with the present investigation, represent a series of studies that have been carried out with a set of utilities based on Open-FOAM. To the authors' knowledge, these are the only CFD simulations of scroll machines performed with open-source software. The results testify the reliability that open-source software have gained over the last years.

2. CFD simulations of scroll compressors

The CFD simulations presented in this article have been performed within the OpenFOAM-v2006 framework. This open-source software is constituted by a set of C++ libraries, including the implementation of different solvers suitable for the study of PD machines, thanks to the availability of compressible flow solver, Arbitrarily Coupled Mesh Interfaces (ACMIs) [19] and dynamic mesh treatment.

Fadiga et al. [17] extended the capability of the software, by developing a series of utilities to generate structured meshes for scroll-type machines and to perform moving mesh simulations based on user-defined nodal displacements. These methodologies, combined with the built-in OpenFOAM mesh generator *snappyHexMesh*, have been employed in this work for creating, manipulating and moving the computational mesh. The OpenFOAM solver adopted by the authors is *rhoPimpleFoam*, a pressure-based segregated solver for transient compressible flows.

2.1. Deforming geometry and mesh motion

The orbital movement of the rotor leads to a change in the solution domain due to the displacement of the solid boundaries. Consequently, the grid nodes have to move to accommodate such displacement, resulting in the introduction of the relative velocity in the convection terms of the Navier-Stokes equations. As an example, this modification is reported for the integral form governing equation of a general tensorial property, Φ:

$$\frac{d}{dt}\int_V \rho\Phi\, dV + \int_S \rho\Phi(\mathbf{u}-\mathbf{u}_S)\cdot\mathbf{n}\, dS - \int_S \Gamma\nabla\Phi\cdot\mathbf{n}\, dS = \int_V q_\Phi\, dV \tag{1}$$

where V is an arbitrary moving volume, S is the surface bounding V, ρ is the density, $\mathbf{n}$ is the outward pointing unit normal vector, $\mathbf{u}$ is the fluid velocity, $\mathbf{u}_S$ is the velocity of the boundary surface, Γ is the diffusivity and q_Φ is the volume source of Φ. Demirdžić and Perić [20] suggest that in order the mesh deformation to respect continuity, the Space Conservation Law (SCL), which describes the conservation of space in case of moving or deforming cells, should be strictly respected. This law is based on the principle that the sum of volume fluxes through cell faces

must correspond to the volume rate of change:

$$\frac{d}{dt}\int_V dV + \int_S \mathbf{u}_S \cdot \mathbf{n}\, dS = 0 \tag{2}$$

Ferziger and Perić [21] illustrate one of the most common methods to satisfy the SCL and ensure mass conservation, which is also implemented in OpenFOAM. This method is based on the calculation of the volumes swept by each cell face over a single time step, which are employed to evaluate the volume fluxes avoiding to explicitly define the grid lines velocities (using these last quantities can easily lead to errors).

In this work, the orbiting motion of the mobile scroll is handled using a user-defined nodal displacement technique. This method is based on the generation of a set of structured grids corresponding to a number of angular positions predefined by the user. The nodal positions are stored and serve as guidelines for the mesh nodes during the scroll revolution, with the option of linearly interpolate between successive grids to adopt arbitrary time steps, which are constrained in accordance with a user-defined threshold of Courant-Friedrichs-Lewy (CFL) number calculated at the end of every time step. This procedure, extensively described in [17], is in accordance with the theoretical basis described in the previous paragraphs of this section.

On the other hand, the key-frame re-meshing method includes a mesh replacement for each time step, leading to possible infringements of the SCL, as reported by Rane et al. [22]. Another method that does not involve motion of the mesh, but is suitable for the correct replication of the scroll operation is the Cut-Cell method, as presented in [11]. Such an approach involves the generation of a background Cartesian grid in which the geometry to be investigated is contained. In correspondence of the walls, the mesh is adapted to represent the boundary, and the cells falling into the "solid" part of the scroll are discarded. In the framework of the cut-cell method, the space conservation law is not automatically respected, as reported in [23]. A non-trivial treatment is required to enforce the mass conservation that follows from such volume mismatch.

2.2. Compressible flow and real gas properties

In PD machines, the fluid density is strongly influenced by its pressure. Density variations, which must be considered in the numerical analysis, are triggered by two different phenomena. Firstly, supersonic or transonic leakage flows develop in gap regions, which can be thought of as convergent-divergent nozzles. Additionally, chamber volumes are subjected to considerable variations to achieve compression or expansion of the operating fluid.

In the present analysis, the large part of the domain presents little compressibility, hence the authors have decided to adopt a pressure-based solver, trying to reach higher accuracy in low-Mach regions. The thermophysical properties have been evaluated using the native OpenFOAM implementation of the Peng-Robinson EOS, associated with polynomials models for transport properties. This decision is supported by the findings of Papes et al. [24] and Fadiga et al. [25, 26], who have investigated the real gas modelling in CFD simulations with refrigerant fluids.

2.3. Leakages and sealing

Internal leakages represent a phenomenon that is inherently included in scroll compressors. Considering that the gap sizes are usually below 100 µm, even small variations can produce non-negligible effects on the volumetric efficiency of the compressors. Such variations can be caused by heating and cooling phenomena linked to the compression process, as well as mechanical loading. An additional aspect to be considered is the presence of tip sealing components, which reduce axial leakages. The sealing capacity of tip seals is not constant, since friction and wear influence the mass flow rate of refrigerant. Modelling all these aspects would require a wide range of complex computational methodologies, ranging from Fluid Structure Interaction (FSI)

to special treatments for thermal deformation and tip seals efficiency. However, it is possible to reach good levels of accuracy by setting a constant gap size, which can be tuned with the help of experimental data. When structured grids are adopted that gap modelling is naturally included as the mesh is squeezed with little quality degradation. In this work, the theoretical orbiting radius of the mobile scroll has been slightly reduced to generate a constant flank gap, combined with the assumption of perfect axial sealing.

3. Computational domain and numerical set-up

The scroll compressor analyzed in this work is one of the machines of the *Danfoss SH* compressor family.

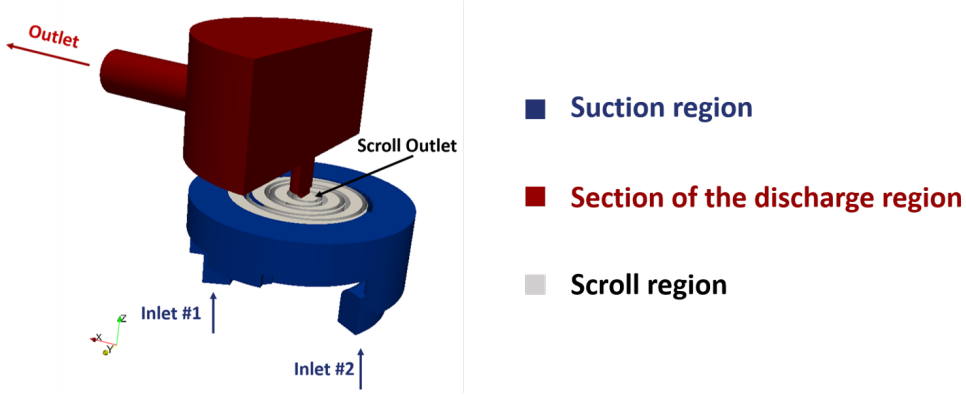

Figure 1. Computational domain of the scroll

The simulations have all been performed in oil-free conditions, although the original compressor works as an oil-flooded machine. The sealing action of the oil has been considered by acting on the flank gap size, while the cooling effects have not been considered. Figure 1 reports the computational domain, consisting in a fixed suction port (blue), a moving mesh region in correspondence of the scroll wraps (grey) and a large reservoir included in the fixed discharge volume (red). While the moving region has been discretized with a structured mesh, in accordance with the methodology reported in section 2, the stationary parts have been meshed with the unstructured mesh generator *snappyHexMesh*. The patch indicated with the name *Scroll Outlet* is an ACMI interface between the moving part and the discharge region. This patch has been used to evaluate the mass flow rate at the machine outlet. The resulting structured mesh is aligned with the software requirements in terms of mesh quality, as confirmed by the OpenFOAM native utility *checkMesh*. More particularly, the gap regions are characterized by regular stretched cells with an aspect ratio of approximately 220, as shown in figure 2.

The representation of the structured grid at an orbiting angle of 0° is reported in figure 2, where the region in correspondence of the end of the mobile spiral has been highlighted. This important area, which is in the proximity of the ACMI interface between the moving domain and the suction port, has been meshed with the aid of a quadratic grading function that reduces the size of the cells in accordance with the local width of the flank gap. The grading function has been applied to the edge reported as *Smoothed edge* in figure 2. This adaptive method has been implemented to improve the accuracy in the computation of the flow in the admission area, avoiding significant differences in the size of adjacent cells. The simulations have run fully parallel on a 40 cores machine, with a computational time of more than four scroll revolutions per 24 computational hours on a mesh with more than 2.5E+06 cells (corresponding to the case with the reservoir). Approximately, 600k and 800k cells have been used to discretize respectively

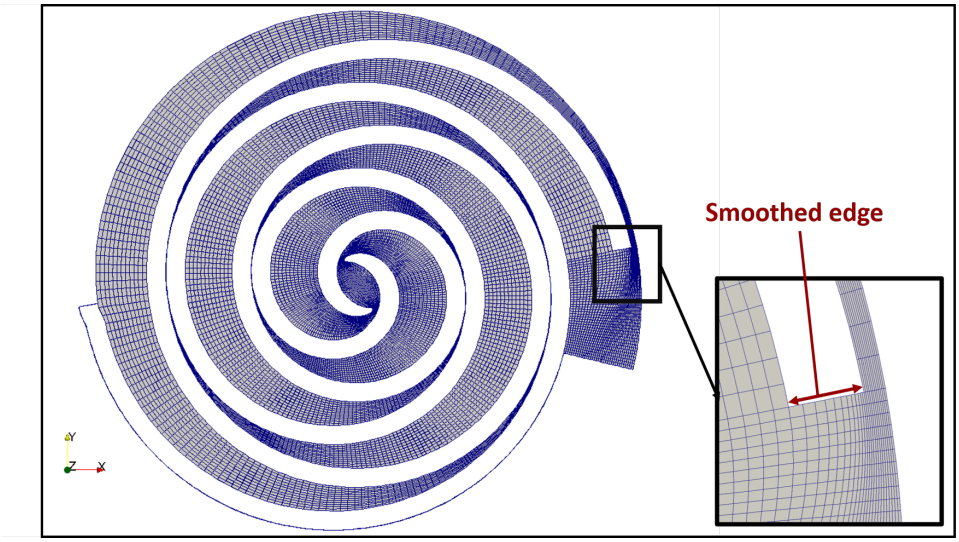

Figure 2. Structured mesh of the moving domain. Highlighted area: adaptive grading of the additional block cells.

the moving and the suction domains. The case with no reservoir, with more than 1.5E+06 cells, runs more than five scroll revolutions per 24 computational hours. The average values of Y-plus calculated at the domain boundaries range from approximately 20 to 400. The highest values have been evaluated at the reservoir walls, where particular accuracy is not required considering the purpose of this work. A grid independence study has not been included in this work, because the mesh size has been chosen according to the authors' experience in similar computational studies performed on scroll machines.

3.1. Simulation campaign

The numerical campaign is characterized by three main analyses, which have been performed on the full computational domain, inclusive of the outlet reservoir. The pressure ratio has been varied to inspect under and over-compression, while keeping the flank gap size at a constant value of 60 µm. The operating point corresponding to the Air-Conditioning and Refrigeration Institute (ARI) standard has been taken as reference, with a rotational speed of 2900 rpm. The pressure ratio of the ARI point is multiplied by 1.83 to reach the high PR point, while the low PR condition is set to a pressure ratio corresponding to 51 % of the reference one. The experimental study proposed by Picavet et al. [3] has been employed as validation for the three analyses reported above.

From the first set of analyses, it has been noticed that the presence of a large reservoir in the discharge region produces a low-frequency pressure wave, much lower than the scroll revolution frequency. This phenomenon is the cause of a lack of convergence at the outlet of the computational domain, as highlighted in section 4. Thus, the authors have decided to perform an additional simulation removing the reservoir and adding a non-reflective boundary condition, in order to isolate the reservoir effects. The last analysis regards the flank gap size: starting from the simulation with no reservoir, the radial distance between the two spirals has been increased from 60 µm to 100 µm.

3.2. Numerical schemes and boundary conditions

Fully turbulent adiabatic simulations employing Menter's k-ω SST model with updated coefficients have been performed. A second-order discretization scheme has been applied to

spatial and time-dependent terms, with the exception of turbulent quantities. Furthermore, gradient limiters have been necessary to ensure the stability of the analyses.

The boundary conditions imposed for the full domain cases include fixed static pressure at inlet and outlet and inflow conditions based on specified mixing length for turbulence specific dissipation. The turbulent kinetic energy is evaluated at inlet and outlet, in case of inflow, according to a user-supplied turbulence intensity value. Temperature values have been imposed in case of flows entering the domain, while zero gradient conditions have been applied on outflows. It is particularly important to take care of reverse flow both at inlet and outlet because it is an inherent phenomenon in positive displacement machines, especially in the case of under-over compression. Accordingly, the velocity boundary conditions have been set as follows: for the flow leaving the domain, a zero gradient condition has been applied. On the other hand, for the flow entering in the domain a velocity value based on the flux in the patch-normal direction has been imposed. Lastly, for the simulations performed with the modified discharge port, with no reservoir, the outlet boundary conditions on velocity and pressure have been replaced with the OpenFOAM native implementation of non-reflective boundary conditions.

4. Results

Table 1 contains values of power and mass flow rate averaged over a complete revolution of the compressor. It is interesting to notice how the presence of the reservoir generates an imbalance between the inlet and outlet mass flow rate. The reason is clearly represented in figure 3, where the different periodicity of the mass flow rate trend at the domain outlet (*Outlet*) is highlighted. The pressure waves that produce this mass flow rate trend is influencing also the region in proximity of the scroll outlet, increasing the time needed to reach an acceptable level of convergence. These issues are the main reasons behind the decision of performing an additional simulation with no reservoir.

	$\dot{m}_{in}/\dot{m}_{in,ARI}$	$\dot{m}_{out}/\dot{m}_{in,ARI}$	$\dot{m}_{out}/\dot{m}_{in}$	VE
ARI	1.0	1.017	1.017	0.967
HP	0.381	0.396	1.039	0.941
LP	1.214	1.213	0.9991	0.975
ARI NR	1.002	1.005	1.003	0.969
ARI NR 100 µm	0.941	0.948	1.007	0.910

Table 1. Revolution-averaged mass flow rate, mass imbalance and volumetric efficiency. (NR = No Reservoir, $\dot{m}$ = Mass Flow Rate, VE = Volumetric Efficiency).

The pressure trend during the compression process is very well captured for all the operating conditions. In this work, the *direct* chamber is the compression chamber which firstly opens towards the discharge port, while *indirect* refers to the other. In figures 4, 5, 6 and 7, *pDirect* and *pIndirect* refer to the pressure recorded in the direct and indirect chambers. *pSuction* is the pressure recorded by a probe in the suction region, while *pDischarge* has been evaluated in the discharge region. Lastly, *pExDir* and *pExInd* are the experimental trends collected by Picavet et al. [3], respectively for the direct and indirect chamber.

ARI: the pressure trend (figure 4) is accurately reproduced, especially in the second half of the compression process. There is a small overestimation of the two peaks that occur in the discharge phase. This difference is probably due to the absence of tip seals in the final part of the scroll wrap (not modelled in this work), as reported in [3].

High pressure ratio: The under-compression generates reverse flow as the discharge port opens (figure 5). The consequent pressure peaks are very well captured by the numerical simulation. This validation is important as it is not highly influenced by the gap sizes. On

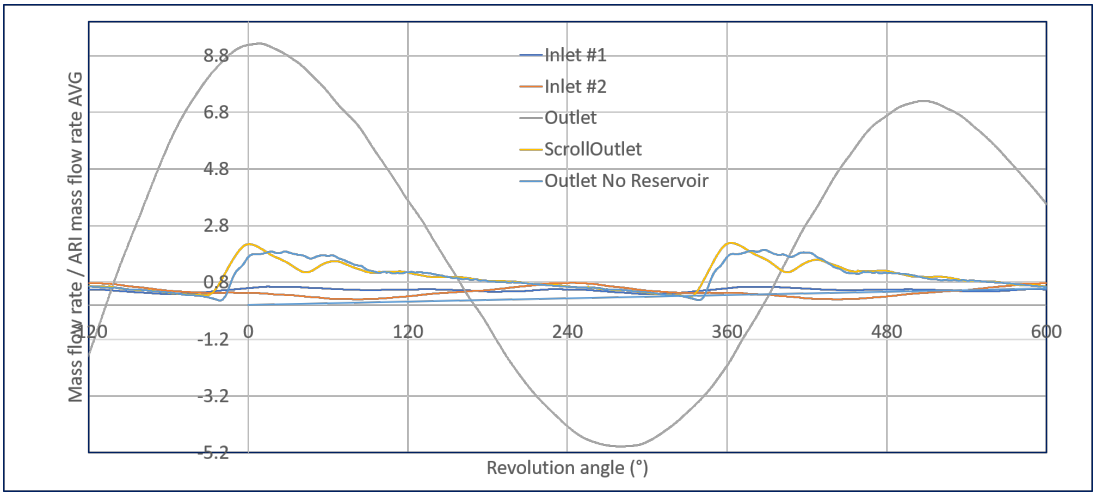

Figure 3. Mass flow rate as a function of the revolution angle. ARI point. Mass flow rate values have been divided by the revolution average of the inlet mass flow rate at ARI conditions (with reservoir).

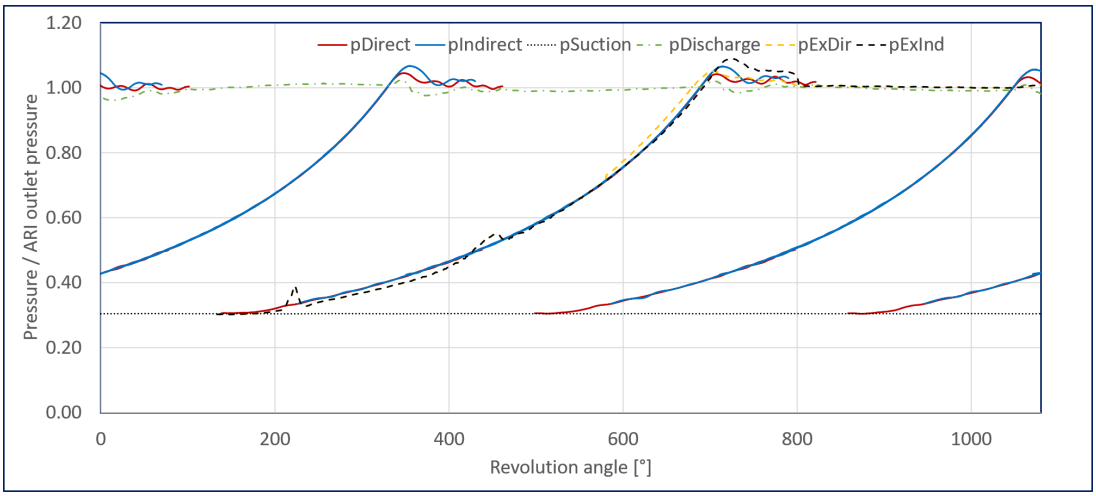

Figure 4. Pressure trends as functions of the revolution angle. ARI. Pressure values have been divided by the outlet pressure of the ARI point.

the other hand, underestimation of the pressure values can be seen in the final part of the compression. The higher pressure ratio amplifies the effects of the modelling assumptions described in section 2.3.

Low pressure ratio: The most interesting aspect of the low pressure ratio trend (figure 6) is related to the expansion process corresponding to the opening of the compression chamber. The discharge pressure experiences a fast decrease before stabilizing again at the outlet pressure levels. In this case, the peaks of the simulated trends are higher than the experimental data.

4.1. Impact of the reservoir and gap size effects

Regarding the pressure values in the compression chambers, the absence of the reservoir does not produce significant variations. Conversely, the removal of the reservoir has a beneficial effect on the global conservation of the mass flow rate. Table 1 highlights a consistent reduction (from

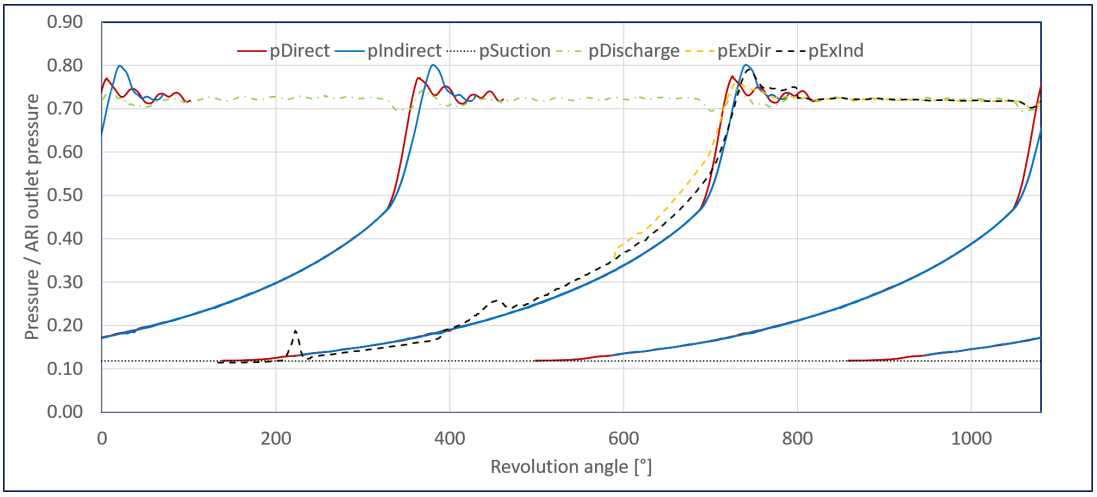

Figure 5. Pressure trends as functions of the revolution angle. High pressure ratio. Pressure values have been divided by the outlet pressure of the ARI point.

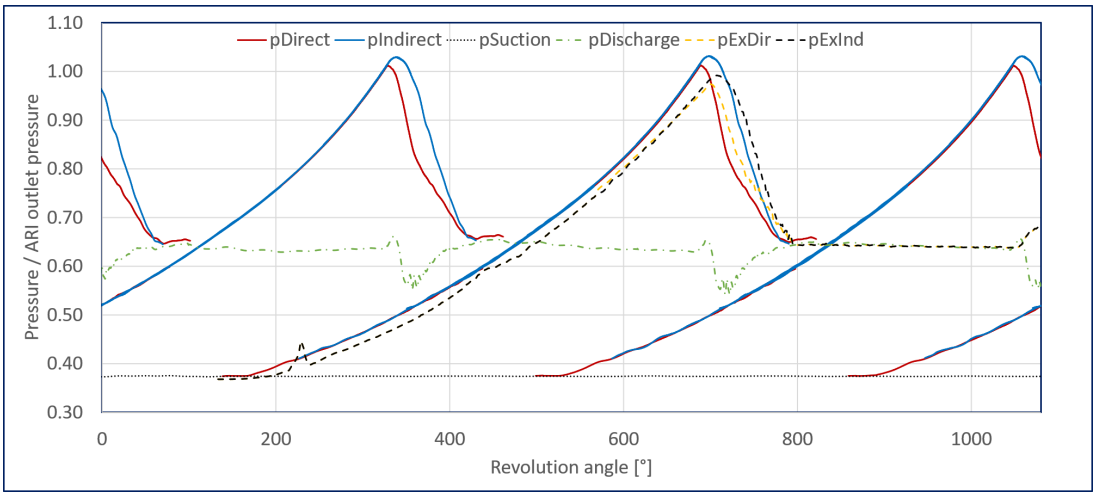

Figure 6. Pressure trends as functions of the revolution angle. Low pressure ratio. Pressure values have been divided by the outlet pressure of the ARI point.

the 1.6 % to the 0.3 %) in the difference between the suctioned and discharged mass flow rate over a complete revolution of the machine. The comparison between the *Outlet* and *Outlet No Reservoir* cases are represented in figure 3. The low frequency oscillations in the mass flow rate trend recorded at the domain outlet have been completely removed by eliminating the reservoir.

The determination of the flank gap size leading to the most accurate solution is certainly a challenging task. The comparison between figure 7 and figure 4 shows that the value of 60 µm produces a solution that is closer to the experimental reference. However, the low pressure ratio and high pressure ratio trends show that there is still room for improvement, probably in the area of the tip region modelling. It is important to underline that the introduction of axial gap modelling requires additional interfaces, which would be placed in regions where cells with high aspect-ratio are needed. This is definitely a topic that should be covered in future developments of the open-source framework for scroll machines presented in this article.

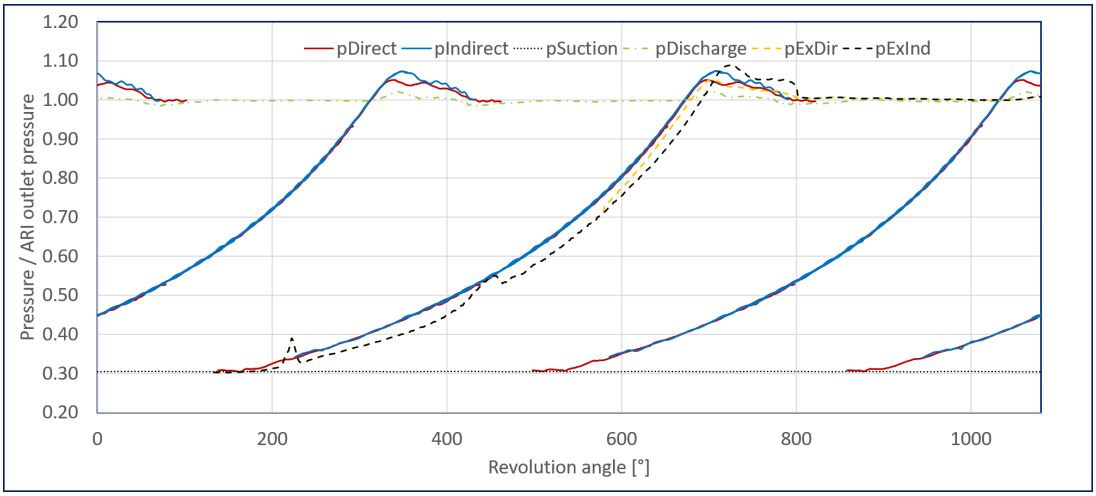

Figure 7. Pressure trends as functions of the revolution angle. ARI point, no reservoir, 100 µm. Pressure values have been divided by the outlet pressure of the ARI point.

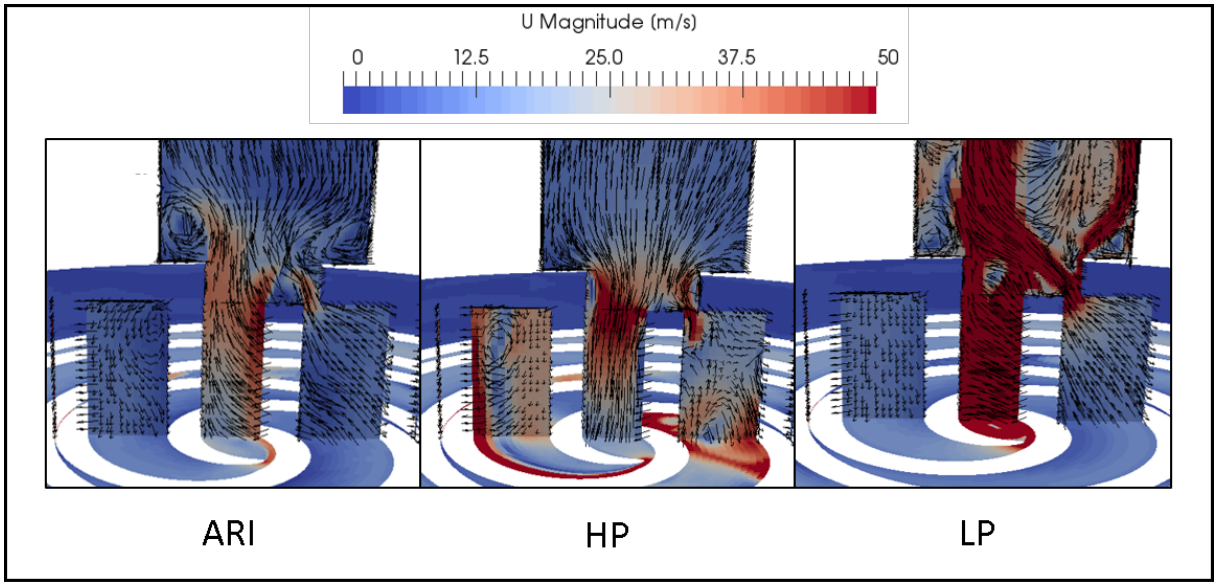

Figure 8. Contour of the velocity magnitude.

4.2. Under and over-compression

The discharge process is represented in the contour of the velocity magnitude (figure 8). There are several fluid dynamics phenomena to be highlighted: in the ARI case, the separation zone downstream the main outlet duct is clearly visible on the left. This phenomenon is strongly amplified when a lower pressure ratio is imposed between outlet and inlet, leading to a jet flow that occurs when the compression chambers open. Lastly, the high pressure ratio case is characterized by a large amount of reverse flow, which enters in the scroll domain influencing also the upstream chambers. The effects of under and over-compression are also reflected in the volumetric efficiency of the compressor, as reported in table 1. The HP case is characterized by a reduction of the volumetric efficiency close to 2.5 %, due to the increased leakages mass flow rate. Overall, the compressor shows good volumetric performance, even in presence of strong

variations in the pressure ratio.

5. Conclusions

The authors have presented the first open-source simulation of a commercial scroll compressor, complete with experimental validation. This achievement could represent a starting point for including new modelling options in the field of positive displacement machines CFD. In fact, open-source frameworks are particularly suitable for the implementation of multiphase models, studies on heat transfer or optimization procedures.

The post-processing highlights the importance of CFD in the analysis of off-design conditions characterized by over and under-compression phenomena. The fluid dynamic behaviour of the compressor during the discharge processes can be analyzed at different operating points, with the possibility of extracting loss coefficients that can be adopted in reduced-order models. Additionally, the flank gap size has been the object of a preliminary analysis, with the aim of evaluating the variations of the pressure trends in the compression chambers, as well as the reduction in the volumetric efficiency.

References

[1] Ramaraj S, Yang B, Braun J, Groll E and Horton W 2014 *International Journal of Refrigeration* **46** 185–195
[2] Bell I, Lemort V, Groll E, Braun J, King G and Horton W 2012 *International Journal of Refrigeration* **35** 1890–1900
[3] Picavet A and Ginies P 2014 Experimental pressure-volume diagrams of scroll compressors *Proc. 22nd Int. Compressor Eng. Conference at Purdue*
[4] Bell I, Groll E, Braun J, Horton W and Lemort V 2014 *International Journal of Refrigeration* **45** 223–242
[5] Gravesen J and Henriksen C 2001 *Society for Industrial and Applied Mathematics* **43** 113–126
[6] Tello-Oquendo F M, Navarro-Peris E, Barceló-Ruescas F and Gonzálvez-Maciá J 2019 *International Journal of Refrigeration* **106** 308–326
[7] Park Y C, Kim Y and Cho H 2002 *International Journal of Refrigeration* **25** 1072–1082
[8] Sung J P, Boo J H and Jung E G 2020 *Energies* **13**
[9] Emhardt S, Tian G, Song P, Chew J and Wei M 2020 *Energy* **199** 117399
[10] Morini M, Pavan C, Pinelli M, Romito E and Suman A 2015 *Applied Thermal Engineering* **80** 132–140
[11] Pham H D, Brandt T and Rowinski D H 2018
[12] Rowinski D H, Li Y and Bansal K 2018
[13] Hesse J, Spille-Kohoff A, Andres R and Hetze F 2018 Cfd simulation of scroll compressors with axial and radial clearances and thermal deformation *18. ISS* pp 123–137
[14] Picavet A and Angel B 2016 Numerical simulation of the flow inside a scroll compressor equipped with intermediate discharge valves *Proc. 23th Int. Compressor Eng. Conference at Purdue*
[15] Picavet A and Genevois D 2018 Three-dimensional navier-stokes simulations of working of scroll compressors *Proc. 24th Int. Compressor Eng. Conference at Purdue*
[16] Cavazzini G, Giacomel F, Ardizzon G, Casari N, Fadiga E, Pinelli M, Suman A and Montomoli F 2020 *Energy* **209** 118382
[17] Fadiga E, Casari N, Suman A and Pinelli M 2020 *Energies* **13(3)** 666
[18] Fadiga E, Casari N, Suman A and Pinelli M 2020 Multi-component numerical investigation of a micro organic rankine cycle *Rankine 2020*
[19] Farrell P and Maddison J 2011 *Computer Methods in Applied Mechanics and Engineering* **200** 89–100
[20] Demirdžić I and Perić M **8** 1037–1050
[21] Ferziger J H and Perić M 1999 *Computational Methods for Fluid Dynamics* 2nd ed (Berlin: Springer)
[22] Rane S, Kovacevic A, Stosic N and Kethidi M **36** 1883 – 1893
[23] Bennett W, Nikiforakis N and Klein R 2018 *Journal of Computational Physics* **368** 333–358
[24] Papes I, Abdelli L, Degroote J and Vierendeels J 2015 3d cfd analysis of a twin screw expander with different real gas models for r245fa *ASME 2015 Int. Mechanical Engineering Congr. and Exp.* p V07AT09A045
[25] Fadiga E, Casari N, Suman A and Pinelli M 2020 *Computer Physics Communications* **250** 107047
[26] Fadiga E, Casari N, Suman A and Pinelli M 2020 Fluid thermophysical properties modelling in an opensource platform: Coolfoam *ECOS 2020*